Effect of Contact Line Pinning on Maximum Spreading of Liquid Drop Impacted onto Groove-Textured Surfaces

V. Vaikuntanathan*, D. Sivakumar
Department of Aerospace Engineering, Indian Institute of Science, Bangalore 560 012, INDIA
visakh@aero.iisc.ernet.in and dskumar@aero.iisc.ernet.in

Abstract

The present work attempts to develop an understanding on the role of contact line pinning on roughness asperities of target surfaces in the maximum spreading diameter of an impacting liquid drop. Model rough (textured) surfaces of stainless steel material comprising unidirectional parallel grooves were used as the target surfaces. The impacted drop spreading in the direction perpendicular to the grooves experiences the pinning of its contact line as the drop liquid advances over the asperity posts. The highlight of the current study is the modeling of this contact line pinning as an energy loss parameter in terms of the contact angle hysteresis of liquid drop on the target surfaces, and its inclusion in the energy conservation based theoretical models of maximum spreading diameter. Experimental measurements of maximum spreading diameter of impacting drops of water and ethanol-water mixture with varying Weber number (~ 2 to 80) were collected on three groove-textured surfaces with different groove depths and pillar angles. The model predictions clearly capture the experimental observation of a reduction in maximum drop spreading in the direction perpendicular to the grooves compared to that on smooth surface and its trend with *We* for all the drop impact cases studied here. A comparison of the model predictions of maximum spreading diameter of impacting liquid drop perpendicular to the grooves with the experimental data yielded satisfactory quantitative agreement with a maximum error of ~14%. Further, in the limiting case of zero roughness, the model reduces to the one for maximum drop spreading during drop impact on smooth surfaces reported by Ukiwe and Kwok.

1. Introduction

The phenomenon of liquid drop impact on solid surfaces is ubiquitous in industrial applications (fuel spray drops impacting on combustion chamber wall in aircraft engines and on piston head in internal combustion engines; spray painting/coating and cooling applications [1]; ink drops impacting on a paper surface in inkjet printing [2], pesticide spraying on leaf surfaces [3], etc.) as well as in nature (rain drops impacting on the surfaces of plant leaves) and our everyday life (rain drops impacting on windshield of automobiles). An understanding of the physical mechanisms governing liquid drop impact process is essential in understanding and beneficially modifying some of the above-mentioned industrial applications. This serves as a clear motivation behind the recently renewed interest in drop impact related studies.

A liquid drop impacting onto a solid surface typically undergoes most of the following sequential processes: spreading radially outward from the impact point till a maximum spread is achieved, at constant contact diameter contact angle decreases till the receding contact angle is attained, receding towards the impact point, contact angle oscillations at constant contact diameter till an equilibrium configuration is reached (Fig. 1). Energetically, a part of the initial kinetic energy of the impacting liquid drop is converted into surface energy and the rest is lost in the form of viscous dissipation during the spreading process [4]. On reaching the maximum spreading, the drop possesses mostly surface energy a part of which is converted back to kinetic energy and the rest lost as viscous dissipation during the receding process. Finally, the viscous losses associated with contact angle oscillations make the drop to attain an equilibrium configuration on the solid surface.

The maximum spreading, quantified by the maximum contact diameter, D_m, of liquid drop impacting onto a solid surface is a direct indicator of the maximum area of the solid surface that is wetted by the drop liquid under a given drop impact condition. This is one of the significant parameters which directly affects the drop impact outcome in many of the afore-mentioned practical applications. For example, predicting the degree of cooling of heated surfaces in spray cooling applications requires knowledge of the area of surface wetted by impacting coolant drop [1]. However, most of the conventionally machined solid surfaces encountered in practical applications exhibit roughness in the form of micro-/nano- asperities and grooves [5]. A liquid drop impacting on such a rough solid surface encounters pinning of its spreading contact line at the edges of roughness asperities. The additional resistance experienced by the spreading liquid drop in the form of contact line pinning may result in a reduced maximum spreading of the impacting drop on rough solid surfaces.

* Corresponding author: visakh@aero.iisc.ernet.in

A survey of the current literature indicates a serious lack of understanding in the maximum spreading of liquid drops impacting rough solid surfaces. However, a lot of research attempt in the form of experimental, analytical, and computational investigations has gone into understanding the maximum spreading of liquid drops impacting smooth solid surfaces (refer to [6] and references therein). Most of the theoretical models developed to predict the maximum drop spreading were based on the principle of conservation of energy applied to the liquid drop impacting on smooth solid surfaces [7]-[13]. Roisman et al. [14] used a combination of mass and momentum conservation applied to the rim of liquid drop and energy balance to predict the temporal variation of contact diameter of liquid drops impacted on smooth, flat, and dry solid surfaces. Because of the randomness in the distribution and geometry of roughness asperities on a conventional/randomly rough surface, a meaningful understanding of the role played by the geoemtrical parameters of the asperities in maximum spreading of a liquid drop impacted onto them is quite difficult. Keeping this in mind, many research groups have focused on liquid drops impact onto textured surfaces comrpising a uniform distribution of geometrically well-defined roughness asperities (refer to [6] and references therein). However, research attempts in explaining the observations on maximum drop spreading on textured surfaces seem non-existent. Recently, Lee and Lee [15] modeled the maximum spreading of liquid drops impacting micro-porous, textured surfaces by taking into account the state of liquid drop (Wenzel or Cassie) on the surface. Moreover, the effect of contact line pinning at the edges of roughness asperities in maximum drop spreading during impact on textured surfaces is not addressed in the current literature eventhough the concept of drop contact line pinning has been addressed in other contexts (refer to [16] and references therein). For example, studies on liquid drops suspended on top of single asperities in the form of square, frustoconical, and rectangular posts pointed out that the drop contact line gets pinned at the asperity edges and will undergo a de-pinning event only when the drop contact angle becomes equal to $\theta_a + \psi$, referred to as Gibbs' criterion, where θ_a is the drop advancing contact angle on smooth surface, and ψ is the local inclination angle of the asperity's side [17], [18].

The current study is an attempt to abridge this gap in the understanding of maximum spreading of liquid drops impacted onto textured surfaces. Parallel groove-textured surfaces are chosen as target surfaces in the current study as they are an apt choice representative of real surfaces on which groove-like features are omnipresent [5]. The details of the theoretical model are outlined in Section 2. Section 3 focuses on the experimental methodology adopted to arrive at the measurements of maximum drop spreading to validate the theoretical model. Section 4 deals with the results arrived at from the experimental study, their comparison with the theoretical predictions, and related discussion. The paper concludes with a summary of the main findings of current study.

2. Theoretical Model

The theoretical model to be presented here is based on the principle of conservation of energy applied between two drop states – one just prior to impact onto the target surface (to be referred to with a subscript *i*), and the other at the maximum spreading configuration on the target surface (to be referred to with a subscript *m*) (Fig. 1). The first part of this section will focus on briefly describing the procedure adopted in modelling the maximum spreading of a liquid drop upon impact on a smooth solid surface [11]. The second part of this section will be devoted to explaining the concept of contact line pinning and, mainly, how it is taken into account in the model for predicting maximum spreading of a liquid drop upon impact on a textured solid surface. This section will conclude by presenting the new theoretical model equations for predicting maximum spreading of a liquid drop perpendicular to the grooves upon impact on a groove-textured solid surface.

2.1 Energy conservation based model: Drop impact on smooth surfaces

The total energy of the liquid drop-solid surface system just prior to drop impact on the solid surface, E_i should be greater than the total energy of the liquid drop-solid surface system when the liquid drop is in the maximum spreading configuration, E_m by an amount equal to the viscous energy dissipation during the drop spreading, E_v.

$$E_i = \left(\frac{\pi}{12}\rho D_o^3 U_o^2\right) + \left(\pi\sigma D_o^2\right) + \left(\gamma_{SV} A\right) \tag{1}$$

The first term in the above equation is the kinetic energy of the impacting drop, the second term is the liquid-vapor interfacial energy of the liquid drop, and the third term is the solid-vapor interfacial energy just prior to drop impact on the solid surface. A is the total surface area of the solid, D_o and U_o are drop diameter and velocity just prior to impact on solid surface, ρ is the density of drop liquid, σ is the surface tension of drop liquid, and γ_{SV} is the solid-vapor interfacial tension. The drop configuration at maximum spreading is assumed to be a circular disc of diameter D_m and thickness, h (see Fig. 1(b)). Then, the total energy of the liquid drop-solid surface system at the maximum drop spreading configuration can be expressed as follows:

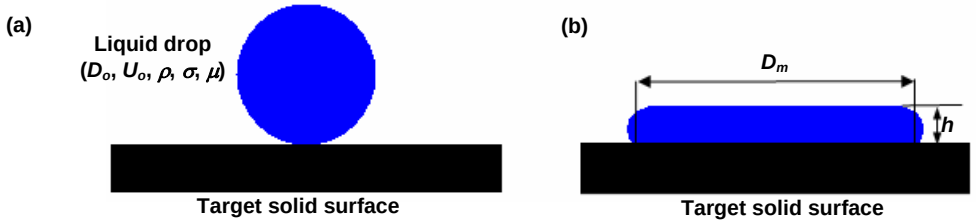

Fig. 1 A schematic sketch of the states of a liquid drop **(a)** just prior to impact, and **(b)** at the maximum spreading on a target solid surface.

$$E_m = \left(\frac{\pi}{4}D_m^2 + \pi D_m h\right)\sigma + \left(\frac{\pi}{4}D_m^2\right)\gamma_{SL} + \left(A - \frac{\pi}{4}D_m^2\right)\gamma_{SV} \tag{2}$$

Here γ_{SL} is the solid-liquid interfacial tension. The viscous energy dissipation during the drop spreading is calculated by taking into consideration the boundary layer of a stagnation point flow model [7], [9].

$$E_v = \frac{\pi}{3\sqrt{\mathrm{Re}}}\rho U_o^2 D_o D_m^2 \tag{3}$$

Re is the Reynolds number defined as follows.

$$\mathrm{Re} = \frac{\rho U_o D_o}{\mu} \tag{4}$$

μ is the dynamic viscosity of drop liquid.

Now, applying the energy conservation principle using equations (1)-(3) gives the following

$$(We + 12) = \left[3\left(1 - \frac{\gamma_{SV} - \gamma_{SL}}{\sigma}\right) + \frac{4We}{\sqrt{\mathrm{Re}}}\right]\beta_m^2 + \frac{12 D_m h}{D_o^2} \tag{5}$$

β_m, the maximum spread factor, is D_m normalized with D_o, and *We* is the Weber number defined as follows.

$$We = \frac{\rho U_o^2 D_o}{\sigma} \tag{6}$$

The thickness of the liquid drop at maximum spreading, *h* can be calculated by equating the volume of the liquid drop just prior to impact to that at maximum spreading configuration which yields the following relation.

$$h = \frac{2}{3}\frac{D_o^3}{D_m^2} \tag{7}$$

Further, the Young's contact angle of the liquid drop on a smooth solid surface, θ_Y is expressed as

$$\cos\theta_Y = \frac{\gamma_{SV} - \gamma_{SL}}{\sigma} \tag{8}$$

Using Eq. (7) and Eq. (8) in Eq. (5) yields the following simplified equation [11].

$$\left[3(1 - \cos\theta_Y) + 4\frac{We}{\sqrt{\mathrm{Re}}}\right]\beta_m^3 - (We + 12)\beta_m + 8 = 0 \tag{9}$$

Equation 9 is based on a more correct modeling approach compared to other models (refer to [11] and references therein) as it takes into account the solid-liquid interfacial energy of the drop at its maximum spreading configuration. The above cubic equation in β_m can be solved to obtain the maximum spread factor, β_m of liquid drops impacting on smooth solid surfaces as a function of the impact conditions.

2.2 Effect of contact line pinning: Drop impact on textured surfaces

On a given textured surface and for a given drop liquid, depending on the drop impact velocity, the liquid drop can take one of the maximum spreading configurations as shown in Fig. 2(b) [19]. Other drop configurations, depending on the number of roughness asperities/grooves filled by the drop liquid, are also possible. The intermediate drop configuration is representative of all such drop configurations with partially-filled roughness asperities/grooves on the textured solid surface.

In order to predict the maximum spread factor in the case of drop impact onto a textured surface, the principle of conservation of energy, as outlined in the first part of this section, is followed. The viscous energy dissipation as modeled by Eq. (3) is assumed to be valid for the case of drop impact on textured surfaces also (any alteration in drop liquid boundary layer characteristics due to solid surface texture is neglected in this analysis). However, the total surface energy of the liquid drop at the maximum spreading configuration (Eq. (2)) is different in this case due to the presence of the surface texture. Further, it depends on whether the liquid drop is in Cassie-Baxter, intermediate, or Wenzel configuration at maximum spreading. Here, the extreme cases of Cassie-Baxter and Wenzel drop configurations at the maximum spreading are considered.

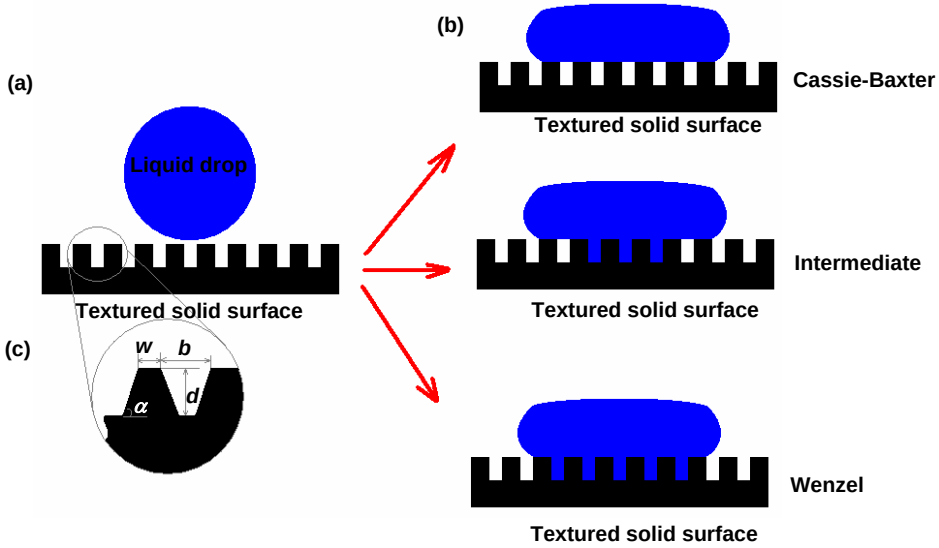

Fig. 2 A schematic sketch of the states of a liquid drop **(a)** just prior to impact, and **(b)** at the maximum spreading on a textured solid surface. **(c)** The geometrical parameters of the textured solid surface.

The total energy of the liquid drop-solid surface system at the maximum drop spreading configuration for the Cassie-Baxter ($E_{m,C}$) and Wenzel ($E_{m,W}$) cases can be expressed mathematically as follows:

$$E_{m,C} = \left[\frac{\pi}{4}D_m^2 + \pi D_m h + (1-\varphi)\frac{\pi}{4}D_m^2\right]\sigma + \left(\frac{\pi}{4}D_m^2\varphi\right)\gamma_{SL} + \left(A - \frac{\pi}{4}D_m^2\varphi\right)\gamma_{SV} \tag{10}$$

$$E_{m,W} = \left(\frac{\pi}{4}D_m^2 + \pi D_m h\right)\sigma + \left(\frac{\pi}{4}D_m^2 r\right)\gamma_{SL} + \left(A - \frac{\pi}{4}D_m^2 r\right)\gamma_{SV} \tag{11}$$

In the above equations, ϕ is the solid fraction of textured surface defined as the fraction of the flat projected area of the textured surface occupied by solid pillars, and r is the roughness factor of textured surface defined as the ratio of the actual area to the flat projected area of the textured surface. They can be mathematically expressed as follows.

$$\phi = \frac{w}{w+b} \tag{12}$$

$$r = 1 + \left[\left(\frac{2d}{w+b}\right)\left(\frac{1-\cos\alpha}{\sin\alpha}\right)\right] \tag{13}$$

Here, w, b, d, and α are the geometrical parameters of the textured solid surface as highlighted in Fig. 2(c).

Now, in the case of a liquid drop impacting on a textured surface, in addition to the viscous energy dissipation, a portion of the drop's initial kinetic energy has to be spent to overcome the drop contact line pinning at the edges of roughness asperities. Contact line pinning occurs due to contact angle hysteresis in which the drop contact line motion will be arrested until the drop contact angle reaches a particular value often referred to as the advancing contact angle. Thus, the energy spent in overcoming the contact line pinning is manifested as an increase in drop contact angle from its dynamic value (here, approximated as equilibrium contact angle) to the advancing contact angle. It is worth stressing here that during this change in drop contact angle, the contact diameter of liquid drop remains constant and hence the energy spent doesn't contribute to the drop spreading process. Hence, this energy is treated as a dissipation to overcome contact angle hysteresis [16]. The following subsection looks into the quantitative treatment of this "pinning" energy loss.

The resistive force due to this contact angle hysteresis acting on the drop contact line per unit length is $\sigma(\cos\theta_r - \cos\theta_a)$ where θ_r and θ_a are the receding and advancing contact angles of the liquid drop on the textured surface respectively (obtained from wetting experiments) [16], [20]. However, when the liquid drop spreads out from the impact point till the maximum spreading configuration it doesn't exhibit any receding and, hence, the receding contact angle is irrelevant in this case. Hence, the contact angle hysteresis force per unit length of the drop contact line is expressed as $\sigma(\cos\theta_e - \cos\theta_a)$ where θ_e is the equilibrium contact angle of the liquid drop on the textured surface obtained from wetting experiments. The drop contact line length over which this hysteresis force per unit length acts varies from zero (at the beginning of impact) to πD_m (at the maximum spreading). It is important to note that any eccentricity in the drop contact line shape at maximum spreading is neglected here. In later sections it will be shown that this is quite a reasonable assumption. Taking an average contact line length of $\pi D_m/2$ over which the hysteresis force per unit length acts on the drop contact line pinned at a pillar edge during the spreading process, the hysteresis force can be expressed as follows.

$$F_h = \frac{\pi}{2} D_m \sigma (\cos\theta_e - \cos\theta_a) \tag{14}$$

The drop contact line has to cross multiple pillar edges from the impact point until it reaches the maximum spreading configuration. The number of pillar edges at which the drop contact line has to de-pin can be expressed as follows.

$$N_p = \frac{D_m}{w+b} \tag{15}$$

Now, the average energy lost by the liquid drop to overcome pinning/hysteresis at pillar edges while spreading from the impact point till the maximum spreading configuration scales as follows.

$$E_p = F_h N_p \frac{D_m}{2} = \frac{\pi D_m^3 \sigma}{4(w+b)} (\cos\theta_e - \cos\theta_a) \tag{16}$$

Applying energy balance, $E_i = E_{m,C}$ (or, $E_{m,W}$) + E_v + E_p (depending on whether the liquid drop is in Cassie-Baxter or Wenzel configuration at maximum spreading), and further simplifying using equations (7), (8), (12), and (13), the following equations for the maximum spread factor of liquid drop upon impact on a textured surface are obtained.

For Cassie-Baxter drop configuration,

$$\left(\frac{3D_o}{w+b}\right)(\cos\theta_e - \cos\theta_a)\beta_m^4 + \left[3\{2-\phi(1+\cos\theta_Y)\} + 4\frac{We}{\sqrt{\mathrm{Re}}}\right]\beta_m^3 - (We+12)\beta_m + 8 = 0 \tag{17}$$

For Wenzel drop configuration at maximum spreading,

$$\left(\frac{3D_o}{w+b}\right)(\cos\theta_e - \cos\theta_a)\beta_m^4 + \left[3(1-r\cos\theta_Y) + 4\frac{We}{\sqrt{\mathrm{Re}}}\right]\beta_m^3 - (We+12)\beta_m + 8 = 0 \tag{18}$$

For drop impact on a smooth solid surface ($\phi = 1$, $r = 1$, $\theta_e = \theta_a$), equations (17) and (18) reduce to Eq. (9). The above model equations are used for predicting the maximum drop spreading perpendicular to the grooves on the target groove-textured surfaces. The contact angles θ_e and θ_a, from here onwards, correspond to the equilibrium and advancing contact angles of the liquid drop perpendicular to grooves (denoted as $\perp$) on the target groove-textured surfaces. It should be noted that the liquid drop front spreading parallel to the grooves (denoted as $\parallel$) does not encounter any pillar edge and, hence, does not experience contact line pinning [21]. However, the effect of freely moving contact line parallel to grooves on β_m in $\perp$ is assumed to be negligible in developing the model equations (17) and (18). This assumption will be justified in Sec. 4.

3. Experimental Methodology

The experimental set up consisted of a liquid drop generator, target surfaces, and a video acquisition system (More details on the experimental set up and its operation can be found in [21]). Distilled water (to be referred to as W) and ethanol-water mixture (5% ethanol by mass; to be referred to as E05) were used as the experimental liquids. The properties of the experimental liquids at ambient atmospheric conditions are given in Table 1. The liquid drop generator consisted of a micrometer-syringe-needle arrangement. The experimental liquid stored in the syringe can be pushed with the help of the micrometer and delivered as an individual drop at the tip of hypodermic needle. The outer and inner diameters of the hypodermic needle were 0.37 mm and 0.25 mm, respectively. The system was capable of delivering W drops of diameter, D_o ~ 2.60 mm (+/- 0.05 mm) and E05 drops of diameter, D_o ~ 2.40 mm (+/- 0.05 mm) with their sphericity (measured just prior to impact) in the range 0.92–1.00. The height of the hypodermic needle tip from the target surface was adjusted to vary the drop impact velocity, U_o.

Table 1 Physical properties of the drop liquids used in the present study.

Experimental liquid	Density, ρ (kg/m^3)	Surface tension (mN/m) [22]	Dynamic viscosity (mPa.s)
Distilled water, W	997	72.01	0.89
Ethanol-water, E05	987	55.73	0.90

The target surfaces used in the present study are parallel groove-textured stainless steel (grade 304) surfaces. Figure 3 shows a typical scanning electron microscopy (SEM) image and surface cross-sectional profile plots of the three groove-textured surfaces. The geometrical parameters, as indicated in Fig. 2(c), of the groove-texture measured from the profile plots, given in Fig. 3(b), are listed in Table 2 along with the wetting characteristics of target surfaces relevant to the theoretical model discussed in the previous section. A smooth (R_a ~ 13 nm) stainless steel surface, RS1 was also used as a reference target surface. It is clear from Fig. 3(b) and Table 2 that the target groove-textured surfaces differed mainly in their groove depth, pillar angle, and, hence, r with almost similar pillar and groove widths and, hence, ϕ. Further, Table 2 also indicates that the wetting characteristics – advancing and equilibrium contact angles measured through captive needle volume addition and sessile drop methods [23], respectively – of a given target groove-textured surface are almost identical for both the drop liquids.

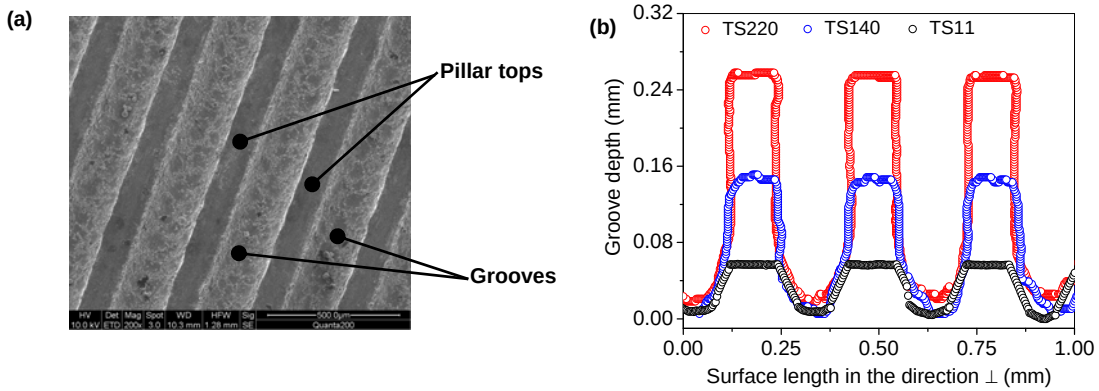

Fig. 3 (a) A typical SEM image (top view) of a target groove-textured surface (TS220), and **(b)** cross-sectional profile plots of the three target groove-textured surfaces used in the present study (adopted from [21]).

The video acquisition system consisted of a high speed digital video camera (Redlake Y4) along with a strobe lamp operated in backlighting mode. The resolution, frame speed, and exposure of the high speed camera were adjusted to capture the details of drop impact process, and the flashing frequency of strobe lamp was synchronized with the operating parameters of high speed camera. The dynamics of drop impacting on target groove-textured surfaces were captured from two elevation views – one for drop dynamics perpendicular to grooves, ⊥ and the other for drop dynamics parallel to grooves, || – through independent experimental runs. Each drop impact experimental run was repeated three times.

Table 2 Geometrical parameters and wetting characteristics of target surfaces.

Experimental liquid	Target surface	Geometrical parameters						Wetting characteristics	
		w (μm)	b (μm)	d (μm)	α (deg.)	r	ϕ	θ_e in ⊥ (deg.)	θ_a in ⊥ (deg.)
Distilled water, W	TS11	116	180	54	42	1.14	0.39	124	132
	TS140	126	173	140	80	1.79	0.42	137	147
	TS220	126	173	220	89	2.45	0.42	135	161
	RS1	R_a ~ 13 nm						76	76
Ethanol-water, E05	TS11	(Same as given above)						124	132
	TS140							136	151
	TS220							136	160
	RS1							71	71

4. Results and Discussion

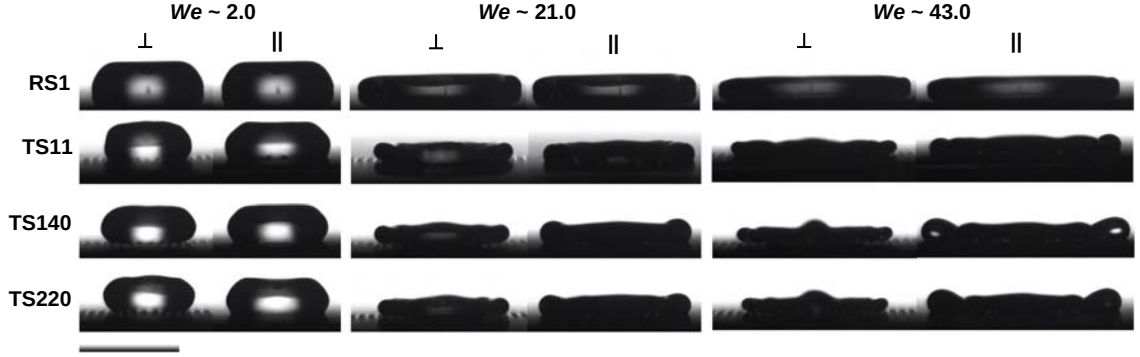

Fig. 4 Images of E05 drops at maximum spreading configuration upon impact onto the target surfaces at three different *We* (impact velocity, U_o). The first and second columns in each *We* case correspond, respectively, to liquid drop front spreading perpendicular and parallel to grooves on target groove-textured surfaces. The horizontal bar shown in the figure corresponds to a length of 3 mm.

Figure 4 shows the maximum spreading configurations of E05 drops impacted onto the target surfaces at three different *We*. As *We* increases (along a row), the maximum drop spreading on target surfaces also increases irrespective of the direction of spreading (⊥ or ||). For a given *We*, the maximum drop spreading perpendicular to grooves on target groove-textured surfaces is observed to be less than that on smooth surface, whereas the maximum drop spreading parallel to grooves is almost similar to that on smooth surface. In order to extract more information, quantitative measurements of maximum drop spreading (shown in Fig. 5) were made using images similar to those given in Fig. 4.

Each plot in Fig. 5 highlights the trend of β_m in ⊥ and || on a groove-textured surface compared to that on the smooth surface with *We*. The plots further strengthen the above-mentioned observation that β_m in ⊥ on all the groove-textured surfaces are less than that on smooth surface. The difference between β_m in ⊥ and on smooth surface is observed to increase with increase in *We*. As *We* increases, the maximum spreading of liquid drop in-

creases. Hence, on a given target surface, the drop front spreading in ⊥ encounters more pillar edges resulting in more energy loss to overcome contact line pinning as proposed in the theoretical model. Further, this difference, especially at higher *We*, is a little more dominantly seen on TS220 and TS140 than on TS11. This is due to a higher advancing contact angle of drop liquid on TS220 and TS140 than on TS11 (see Table 2) which, in turn, can be attributed to a larger pillar side angle of TS220 and TS140 than TS11 [17], [24]. However, there is no significant difference in the trends of β_m in ⊥ with *We* among the target groove-textured surfaces even though they exhibit a considerable difference in their roughness factor, *r* (or groove depth, *d*). It may not be possible to arrive at a clear conclusion on the effect of ϕ on β_m in ⊥ from the experiments on present surfaces.

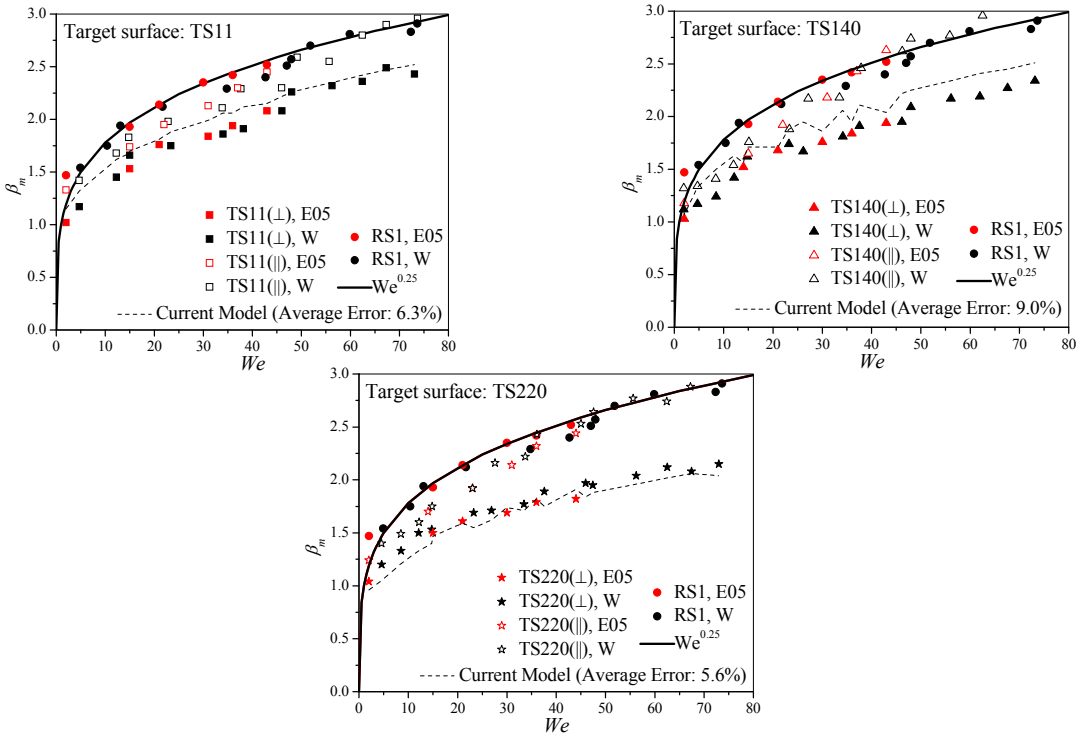

Fig. 5 Variation of normalized maximum spreading, β_m of W and E05 drops impacted on the target surfaces with *We*. Each plot highlights the comparison of β_m in ⊥ and || on a target groove-textured surface with that on smooth surface.

From the plots in Fig. 5 it is clear that β_m in || on all the groove-textured surfaces is almost similar to that on smooth surface, especially at higher *We*. β_m in || on all the groove-textured surfaces and on smooth surface scales with $We^{0.25}$ as proposed by Clanet et al. [10]. Hence, the possibility that the reduced β_m in ⊥ may be due to an enhanced β_m in || relative to smooth surface can be ruled out. The assumption made in the theoretical model that the drop spreading in ⊥ is unaffected by that in || is thus justified here. This, together with the discussion in the previous paragraph, strengthens the proposal of theoretical model that the energy loss to overcome contact line pinning is the primary cause for the reduced β_m in ⊥ on groove-textured surfaces.

Figure 5 also shows plots highlighting the comparison of model predictions with experimental measurements of β_m in ⊥ on target groove-textured surfaces. Based on visual observation from the high speed images of impacting drops, the state of drop – Cassie or Wenzel – was determined, and, accordingly, either Eq. 17 or Eq. 18 was used in model predictions. The average error associated with model predictions are also indicated in each plot. It is evident from the plots that the theoretical model satisfactorily predicts β_m in ⊥ on the groove-textured surfaces used in the present investigation. However, as pointed out earlier, more experiments involving surfaces with a systematic variation in ϕ are required to fully understand the model predictions.

5. Summary and Conclusions

Experiments of drop impact on groove-textured surfaces revealed that the drop front spreading perpendicular to the grooves experiences contact line pinning at the pillar edges whereas that spreading parallel is relatively free of such pinning. This contact line pinning is manifested in experimental observations in the form of a reduction in maximum drop spreading perpendicular to grooves compared to that parallel to grooves and on smooth surface. Modelling of the contact line pinning as an energy loss parameter in terms of contact angle hysteresis of drop liquid on groove-textured surface is proposed in the current study. Further, inclusion of this parameter in the conventional energy conservation based models, together with an appropriate account of surface energy terms due to the presence of texture on solid surface, gave model equations to predict the maximum spreading perpendicular to grooves (β_m in ⊥) of drops impacting on groove-textured surfaces. Satisfactory agreement between the model predictions and experimental measurements of β_m in ⊥ was observed. For the drop impact con-

ditions studied, the model could also predict the trend of β_m in $\perp$ with *We* on three groove-textured surfaces featuring a variation in groove depth and pillar angle. The increase in the difference between β_m in $\perp$ and β_m on smooth surface could be explained as resulting from an increase in the number of pillar edges at which contact line gets pinned and the associated increase in energy loss to overcome contact line pinning as proposed by the model. More experiments involving surfaces with different solid fraction are required to understand its effect on the model predictions.

Acknowledgements
The study has been supported by University Grants Commission, India under the grant Part II-B CAS UGC – Dept. of AE. We would also like to thank Mr. R. Kannan for providing the target surfaces used in the study.

References
[1] Pasandideh-Fard, M., Aziz, S. D., Chandra, S., Mostaghimi, J., "Cooling effectiveness of a water drop impinging on a hot surface", *Int. J. Heat and Fluid Flow* **22** (2001) 201-210.
[2] Asai, A., Shioya, M., Hirasawa, S., Okazaki, T., "Impact of an ink drop on paper", *J. Imaging Sci. Tech.* **37** (1993) 205-207.
[3] Wirth, W., Storp, S., Jacobsen, W., "Mechanisms controlling leaf retention of agricultural spray solutions", *Pesticide Science* **33** (1991) 411-420.
[4] Yarin, A. L., "Drop impact dynamics: Splashing, spreading, receding, bouncing…", *Ann. Rev. Fluid Mech.* **38** (2006) 159-192.
[5] Zhong, Z., "Surface finish of precision machined advanced materials", *J. Mater. Processing Tech.* **122** (2002) 173-178.
[6] Marengo, M., Antonini, C., Roisman, I. V., Tropea, C., "Drop collisions with simple and complex surfaces", *Current Opinion in Colloid & Interface Sci.* **16** (2011) 293-302.
[7] Pasandideh-Fard, M., Qiao, Y. M., Chandra, S., Mostaghimi, J., "Capillary effects during droplet impact on a solid surface", *Phys. Fluids* **8** (1996).
[8] Scheller, B. L., Bousfield, D. W., "Newtonian drop impact with a solid surface", *AIChE Journal* **41** (1995) 1357-1367.
[9] Mao, T., Kuhn, D. C. S., Tran, H., "Spread and rebound of liquid droplets upon impact on flat surfaces", *AIChE* **43** (1997) 2169-2179.
[10] Clanet, C., Beguin, C., Richard, D., Quere, D., "Maximal deformation of an impacting drop", *J. Fluid Mech.* **517** (2004) 199-208.
[11] Ukiwe, C., Kwok, D. Y., "On the maximum spreading diameter of impacting droplets on well-prepared solid surfaces", *Langmuir* **21** (2005) 666-673.
[12] Vadillo, D. C., Soucemarianadin, A., Delattre, C., Roux, D. C. D., "Dynamic contact angle effects onto the maximum drop impact spreading on solid surfaces", *Phys. Fluids* **21** (2009) 122002.
[13] Li, R., Ashgriz, N., Chandra, S., "Maximum spread of droplet on solid surface: Low Reynolds and Weber numbers", *J. Fluids Engg.* **132** (2010) 061302.
[14] Roisman, I. V., Rioboo, R., Tropea, C., "Normal impact of a liquid drop on a dry surface: model for spreading and receding", *Proc. Royal Soc. London A* **458** (2002) 1411-1430.
[15] Lee, J. B., Lee, S. H., "Dynamic wetting and spreading characteristics of a liquid droplet impinging on hydrophobic textured surfaces", *Langmuir* **27** (2011) 6565-6573.
[16] Bonn, D., Eggers, J., Indekeu, J., Meunier, J., Rolley, E., "Wetting and spreading", *Rev. Mod. Phys.* **81** (2009) 739-805.
[17] Extrand, C. W., "Modelling of ultralyophobicity: Suspension of liquid drops by a single asperity", *Langmuir* **21** (2005) 10370-10374.
[18] Semprebon, C., Mistura, G., Orlandini, E., Bissacco, G., Segato, A., Yeomans, J. M., "Anisotropy of water droplets on single rectangular posts", *Langmuir* **25** (2009) 5619-5625.
[19] Bartolo, D., Bouamrirene, D., Verneuil, E., Buguin, A., Silberzan, P., Moulinet, S., "Bouncing or sticky droplets : Impalement transitions on superhydrophobic micropatterned surfaces", *Europhys. Lett.* **74** (2006) 299-305.
[20] de Gennes, P. G., "Wetting: statics and dynamics", *Rev. Mod. Phys.* **57** (1985) 827-863.
[21] Kannan, R., "Experimental study on the impact of water drops on groove-textured surfaces", *Ph. D. Thesis, Indian Institute of Science* (2011).
[22] Vazquez, G., Alvarez, E., Navaza, J. M., "Surface tension of alcohol + water from 20 to 50 ^{0}C", *J. Chem. Eng. Data* **40** (1995), 611-614.
[23] Vaikuntanathan, V., "Dynamics of water drops impacting onto the junction of dual-textured substrates comprising hydrophobic and hydrophilic portions", *M. Sc. (Engg.) Thesis, Indian Institute of Science* (2011).
[24] Fukai, J., Shiiba, Y., Yamamoto, T., Miyatake, O., Poulikakos, D., Megaridis, C. M., Zhao, Z., "Wetting effects on the spreading of a liquid droplet colliding with a flat surface: Experiment and modeling", *Phys. Fluids* **7** (1995) 236-247.